Catena 204 (2021) 105384

Contents lists available at ScienceDirect

Catena

journal homepage: www.elsevier.com/locate/catena

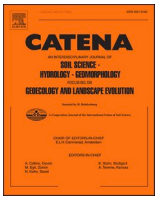

Variable discharges control composite bank erosion in Zoige meandering rivers

Peng Gao [a,*], Zhiwei Li [b,*], Hanyuan Yang [b]

[a] Department of Geography and the Environment, Syracuse University, Syracuse, NY 13244, USA
[b] State Key Laboratory of Water Resources and Hydropower Engineering Science, Wuhan University, Wuhan 430072, China

ARTICLE INFO

Keywords:
Discharge variability
BSTEM
Composite bank erosion
Fluvial erosion
Bank collapse
Hydrograph-based effective discharge

ABSTRACT

This study investigated the roles of variable daily discharges in controlling processes of composite bank erosion in alpine meandering rivers located in the Zoige basin on the Qinghai-Tibet Plateau of China using Bank Stability and Toe Erosion Model (BSTEM). BSTEM was calibrated from compiled daily discharges, field measurements, and pre-determined model parameters for modeling fluvial erosion (FE) and bank collapse (BC) in the lower layer of a conceptualized composite bank profile. Modeling was based on theoretically designed five sets of competent hydrographs, each of which contains seven hydrographs with the same mean daily discharge (Q_a) and variable shapes represented by different combinations of the initial daily discharge, the peak daily discharge, and its occurrence time. The design was guided by 77 real competent hydrographs representing daily discharges recorded in 14 years. Results showed that shapes of these hydrographs (1) had discernable impact on FE and BC, but this impact is secondary to that of Q_a; and (2) affected FE in magnitude, but BC in both magnitude and frequency. After identifying a proportion of the designed hydrographs that are realistic in the existing flow regime, hydrograph-based rating curves for both FE and BC were established and used to create hydrograph-based effective discharges (Q_e) for FE and BC, respectively. Finally, Q_e was correlated to the width of overhanging arm for explaining the dominant processes controlling composite bank erosion and linking the nature of these processes to lateral migration of the associated meandering rivers. This success demonstrates a great potential of using Q_e to reveal many complex processes in fluvial systems.

1. Introduction

Increased incidents of flood events triggered by extreme weather from continuous global warming (Allan and Soden, 2008; Apurv et al., 2015; Giorgi et al., 2019; Hasan et al., 2018; Xu et al., 2019) make our living environment more vulnerable. This raises pressing needs for identifying the dominant flows that alter river morphology for developing and implementing best mitigation measures. The dominant flow traditionally refers to the channel-forming flow expressed as a single magnitude of the discharge controlling river forms and their adjustments (Leopold et al., 1964). Theoretically, this flow captures the balance between frequency and magnitude of a range of flows for achieving the most effective change of channel morphology, which is often termed as the effective or dominant discharge (Knighton, 1998) and is most commonly represented by the effective discharge that transports the highest amount of sediment (suspended, bed, or total) load for a given time period when rivers are in equilibrium (Simon et al., 2016; Wolman and Miller, 1960). It tends to be moderate and relatively frequent in temperate climates and lowlands with less variable flow regimes, whereas may be larger and infrequent in arid and semi-arid climates and headwater areas with highly variable discharges (Knighton, 1998; Wolman and Miller, 1960). The effective discharge often alleges that there exists a single water discharge that most effectively shapes channel forms in a river.

For a long time, determining the magnitude of this discharge has become a canonical rule (Downs et al., 2016; Ferro and Porto, 2012; Goodwin, 2004; Roy and Sinha, 2014; Schmidt and Morche, 2006; Simon et al., 2004; Torizzo and Pitlick, 2004; Wyzga et al., 2020). However, this classic concept is fundamentally rooted in the equilibrium paradigm and hence has encountered a variety of challenges that may be highlighted in two aspects. First, identifying this single discharge requires construction of a flow duration curve using a historical record of discharges and sediment (or nutrient) rating curves. Since processes controlling both river flows and sediment (and nutrient) transport are

* Corresponding authors.
E-mail addresses: pegao@syr.edu (P. Gao), lizw2003@whu.edu.cn (Z. Li).

https://doi.org/10.1016/j.catena.2021.105384
Received 14 August 2020; Received in revised form 11 April 2021; Accepted 13 April 2021
Available online 26 April 2021

strongly nonlinear, different ways of grouping discharge data into classes could lead to different flow duration curves, introducing uncertainties in the determined effective discharge, and poor fitting of sediment data to the statistically significant rating curves may lead to multiple discharges that have comparable capacities of transporting sediment or nutrient loads (Biedenharn et al., 2000; Crowder and Knapp, 2005; Gao et al., 2008; Lenzi et al., 2006). Second, growing studies have divulged a non-negligible influence of discharge variability on shaping channel morphology (Brown and Pasternack, 2014; Esposito et al., 2018; Hooke, 2015; Lotsari et al., 2018; Visconti et al., 2010). Therefore, channel morphology and river ecological functions are indeed controlled by multiple discharges (Doyle et al., 2005). The complexity derived from variable discharges, reflected by the long-standing debate that channel morphology may be shaped by rare flood events (Baker, 1977; Fryirs et al., 2015; Meyer, 2001; Phillips, 2002; Yellen et al., 2016), challenges the conventional assertion of the single-value effective discharge.

The effect of variable discharges on channel morphology appears prominently in erosion processes of river banks whose composition is featured by vegetation-enhanced top layer underlain by a fine sand and/or silt layer with no or much less cohesion (Chen et al., 2011; Dapporto et al., 2003; Micheli and Kirchner, 2002; Samadi et al., 2011). Either near-peak flows or those in the late phase of the flow hydrograph could trigger cantilever failure of composite banks (Luppi et al., 2009; Xia et al., 2014). Mechanisms of fluvial erosion of bank faces and geotechnical failure of the subsequently formed overhanging top bank have been well understood after a large body of studies based on field measurements, laboratory experiments, and numerical modeling for rivers in low and medium altitudes (Chen et al., 2011; Karmaker and Dutta, 2015; Konsuer et al., 2016; Lai et al., 2015; Patsinghasanee et al., 2018; Samadi et al., 2011, 2013). Nonetheless, it is unclear whether similar mechanisms still dominate composite bank erosion in alpine meandering rivers. This uncertainty may lead to a broader and more profound question: whether the impact of variable discharges on erosion of composite banks may be quantitatively characterized in a way similar to the classic effective discharge. Although failure of composite banks could take different modes (e.g., shear, beam, or tensile) (Samadi et al., 2013; Thorne, 1982; Thorne and Tovey, 1981), its occurrence is always episodic compared with consecutive fluvial erosion (Daly et al., 2015; Simon and Collison, 2001). This means that the balance between magnitude and frequency of river flows controlling geotechnical failure of the banks might be drastically distinct from that of the flows dominating fluvial erosion, challenging the existence of a single-value effective discharge for quantifying processes controlling riverbank erosion. Therefore, answering this question may provide new insight into full understand of complex processes controlling composite bank erosion in theory, as well as catalyzing new tools for water resources management in practice.

This study aimed at unfolding how variable discharges may control the two different processes by simulating erosion processes of composite banks in alpine meandering rivers on the Qinghai-Tibet Plateau, China. First, magnitudes of fluvial erosion and bank collapse in these rivers were determined using five sets of theoretically generated competent hydrographs that cover the possible flow variations in the studied rivers. Each set had the same mean discharge (Q_a), but different shapes. The subsequent analyses not only showed that the impact of Q_a on the two processes was greater than that of hydrograph variability, but also led to generation of rating curves for the two processes. These results gave rise to the concept of the hydrograph-based effective discharge that was used to reveal the geomorphological impact and significance of discharge variability on erosion processes.

2. Materials and methods

2.1. Prototype of the composite riverbanks and a cycle of bank erosion

Bank profile and structure for modeling were created in terms of the prototypes of composite banks commonly found in meandering channels within the Zoige basin, which is located on the northeastern side of the Qinghai-Tibet Plateau, China and has elevations ranging between 3400 and 3900 m. The basin is filled with lacustrine deposits consisting of fine sand and silt, forming an average slope of 6.6% running from northwest, south, and southeast to north. It develops two main meandering rivers, Black and White rivers, flowing through the land primarily covered by grassland and peatland and merging into the Upper Yellow River at its first big bend (Fig. 1a and b). The main channels and tributaries of these two rivers are featured by meanders with relatively high sinuosity (Li and Gao, 2019a). A unique phenomenon that has been confirmed by our multi-year field reconnaissance along these meanders is the existence of ubiquitously distributed cantilever riverbanks (Fig. 1c-1e). They are typical composite banks sharing a similar two-layer structure: the upper layer formed by mixture of top soils and roots of grass or peat, and the lower layer consisting of soils with fine sand, silt, and some clays. Yet, field observation and measurement showed that moving from the downstream main reach to the upstream branch, the ratio between the upper and lower layers changes from roughly one fifth to one third. The conceptualized bank profile for modeling was based on the latter (Fig. 1e) because (1) the wadable channel allowed us to survey the cross section for hydraulic calculations, and (2) the channel size is comparable to that in other meandering rivers (Parker et al., 2011), such that results from this study may have broader applications. Specifically, the conceptualized bank profile was based on a reference composite bank in the upstream reach of the Black River (Fig. 1b).

Freeze-thaw processes may promote bank erosion when tension cracks develop on the bank top. Nonetheless, this impact is secondary to fluvial processes, because the latter is the dominant driving force causing the cantilever arm. Fluvial processes shaping the prototype banks follow the erosion cycle of general composite banks (Thorne and Tovey, 1981). Continuous undercutting of the lower layer leads to formation and development of a cantilever till its failure. The cycle completes when failed overhanging blocks are removed by river flows (Ferrel et al., 2018; Patsinghasanee et al., 2018). In river banks whose cantilever layers are mainly comprised of cohesive soil materials, the failed cantilever blocks may break into smaller slumps and be transported away shortly (Eke et al., 2014; Yu et al., 2015), In the Zoige basin, however, the failed soil-vegetation blocks have been observed to stay at the toe of the bank for more than one year before being removed, possibly because these blocks have much stronger cohesion than those without vegetation (Fig. 1e). Furthermore, existing flow regime assures that discharges in meandering rivers within the Zoige basin rarely reach the upper soil-vegetation mixture. Consequently, the rate of overhanging arm development is controlled by the undercutting rate in the lower layer (LL). It follows that the cycle of bank erosion is dominated by undercutting processes in the LL, which may involve (i) continuous fluvial erosion at the bank toe and on the bank face and (ii) episodic mass failure of soil blocks on the upper part of the LL. Although seepage erosion might be an important mechanism of bank erosion in many rivers (Cancienne et al., 2008; Masoodi et al., 2019; Samadi et al., 2013; Simon and Collison, 2001), it is negligible in the prototype rivers for two reasons. First, groundwater flow via bank seepage is very small (Li and Gao, 2019b), such that it hardly causes bank erosion. Second, bank erosion is dominated by relatively high flows that mainly occur in the wet season (i.e., from May to September) during which, seepage flows derived from subsurface and ground flows are much less than storm flows. Therefore, the cycle of composite bank erosion is essentially determined by removal of the LL that is controlled by combination of fluvial erosion and mass failure of the bank face. This cycle ends when cantilever failure of the upper soil-vegetation layer occurs as the

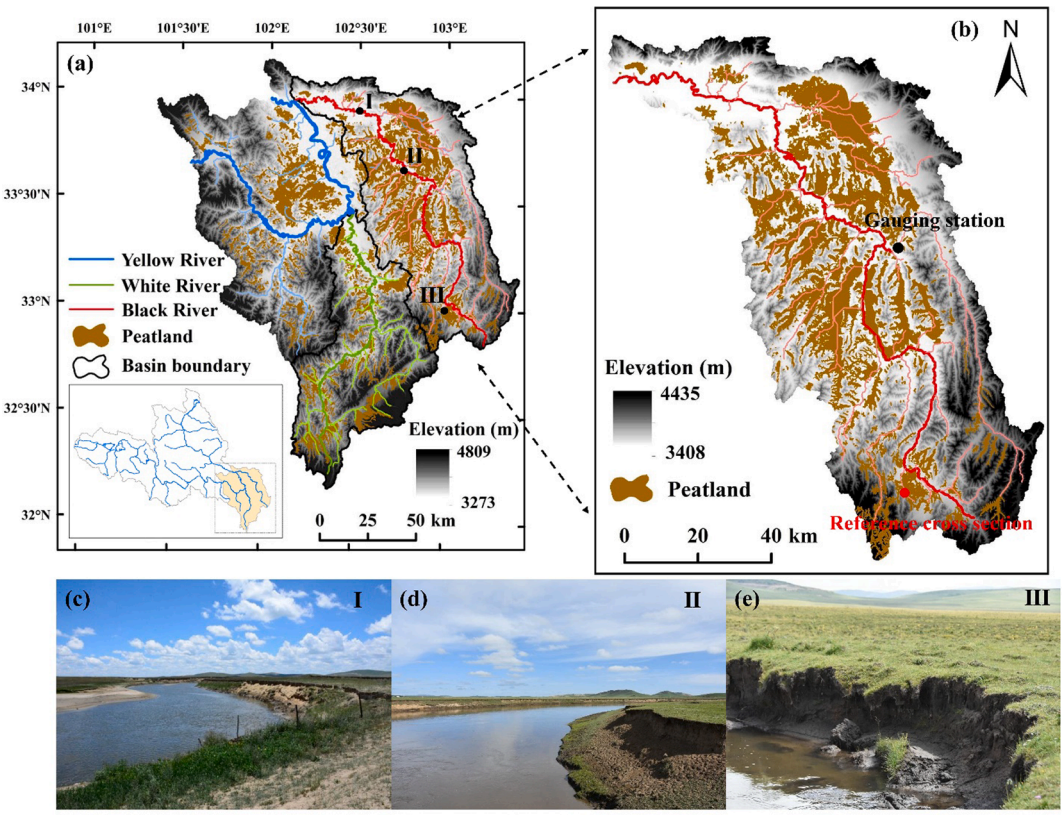

Fig. 1. Study area and prototype rivers. (a) The Zoige basin that holds two meandering river systems (White and Black rivers) on the Qinghai-Tibet Plateau, China. The dark blue line reflects the first bend of the Upper Yellow River. The green line is the main stream of the White River. The red line is the main stream of the Black River, together with three locations where the composite river banks were shown; (b) Locations of the Zoige gauging station and the reference cross section; (c) – (d) the composite banks shown in location I, II, and III marked in (a). (For interpretation of the references to colour in this figure legend, the reader is referred to the web version of this article.)

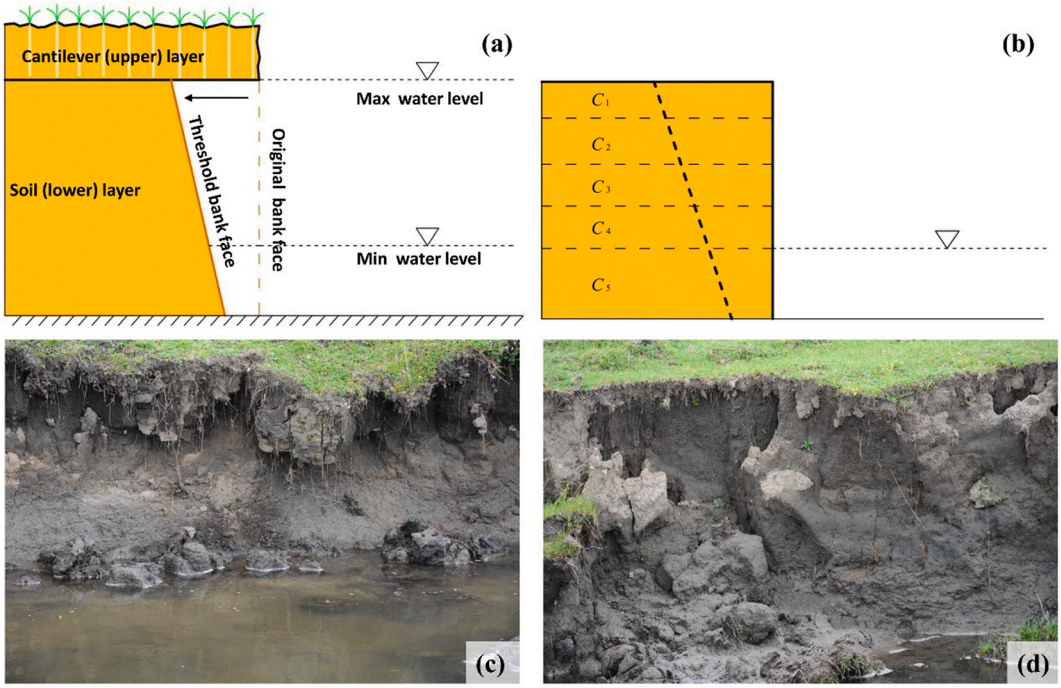

Fig. 2. The conceptual model of the composite bank in prototype rivers. (a) A simplified structure of a composite river bank. The arrow indicates the direction of bank retreat; (b) The conceptual model for BSTEM. The water levels reflect the possible ranges of flows in the reference cross section. (c) – (d) evidence of vertical bank profiles observed in the field.

overhanging arm reaches its threshold value due to removal of the LL. Hereafter, the two modes of undercutting in the LL of a typical composite bank are referred to as fluvial erosion and bank collapse, while cantilever failure is denoted as mechanical failure of the upper soil-vegetation layer.

2.2. Model assumptions

Physical processes controlling erosion of the LL of a typical composite bank were simulated using Bank Stability and Toe Erosion Model (BSTEM). As a widely used model for predicting bank erosion rates (Klavon et al., 2017), BSTEM was adopted here to simulate fluvial erosion using hydraulic equations and bank collapse based on force balance analysis in the LL, though bank erosion could be appropriately described by many other models as well (Chen and Duan, 2008; Guneralp and Marston, 2012; Lai et al., 2015; Motta et al., 2014; Parker et al., 2011; Rinaldi et al., 2008; Samadi et al., 2011).

It should be emphasized that the modeling is not for accurately predicting bank retreat rates in the studied river (Fig. 1b) as many other studies did (Klavon et al., 2017), but for revealing dominant processes that control bank erosion. As such, it is based on several assumptions. First, the above-mentioned cycle of bank erosion applies to composite banks of all channels in the Black River. Thus, model parameters may be calibrated using field measured data around the reference cross section (RCS) (Fig. 1b) and other locations along the Black River. Second, the modeled riverbank profile may be conceptualized as a simplified one based on the RCS that contains two layers, the upper soil-vegetation mixed layer and the lower soil layer (Fig. 2a and 2b). Bank erosion, which include fluvial erosion and bank collapse, starts in the LL and creates an overhanging arm (OA). The failure of the OA is marked by reaching a threshold arm width and the modeling is focused on bank erosion in the LL. The cycle of bank erosion typically begins with a vertical bank profile, which is evidenced by our field reconnaissance along the Black River (Fig. 2c and 2d). Third, the full range of possibly available erosion processes is driven by not only already happened daily discharges, but also those may possibly happen based on existing flow regime. Thus, the recorded daily discharges in the Black River are insufficient to reflect all theoretically possible daily discharges, but may be used to guide the theoretical construction of all possible discharges described later.

2.3. Model calibration

2.3.1. Determination of competent hydrographs using obtained daily discharges

Water discharge is one of the input parameters in BSTEM. However, only limited daily discharges (Q) between 1981 and 2014 are available in a gauging station (i.e., the Zoige station) that is located about 60 km downstream of the RCS (Fig. 1b). They were then converted into Q values at the RCS by multiplying the obtained ones at the Zoige station by a proportional coefficient calculated as the ratio of the contributing areas at the two sites (the Zoige station and the RCS). The contributing areas at the two cross sections are covered by almost uniformly distributed grassland and peatland and their topography is featured by relatively smoothed lacustrine deposits (Fig. 1b). Thus, use of the area-based proportional coefficient for conversion is apparently reasonable (McCuen, 2004). After conversion, Q values were divided into inactive and active components based on the threshold of Q that may initiate fluvial erosion of the bank (Q_t) (Fig. 3a-3c). This means that if a hydrograph representing a storm event is completely below Q_t, then it is an inactive hydrograph, while if a proportion of a hydrograph is below Q_t, then its proportion above Q_t is an active hydrograph, which will be termed as a competent hydrograph. The value of Q_t, which was 0.373 m^3/s, was determined in terms of the critical shear stress described below.

The obtained data missed the middle period of the 34 years between 1981 and 2014. Comparing coefficient of variation (CV) for Q in the wet (i.e., May-October) and dry seasons (i.e., November-April) of each year

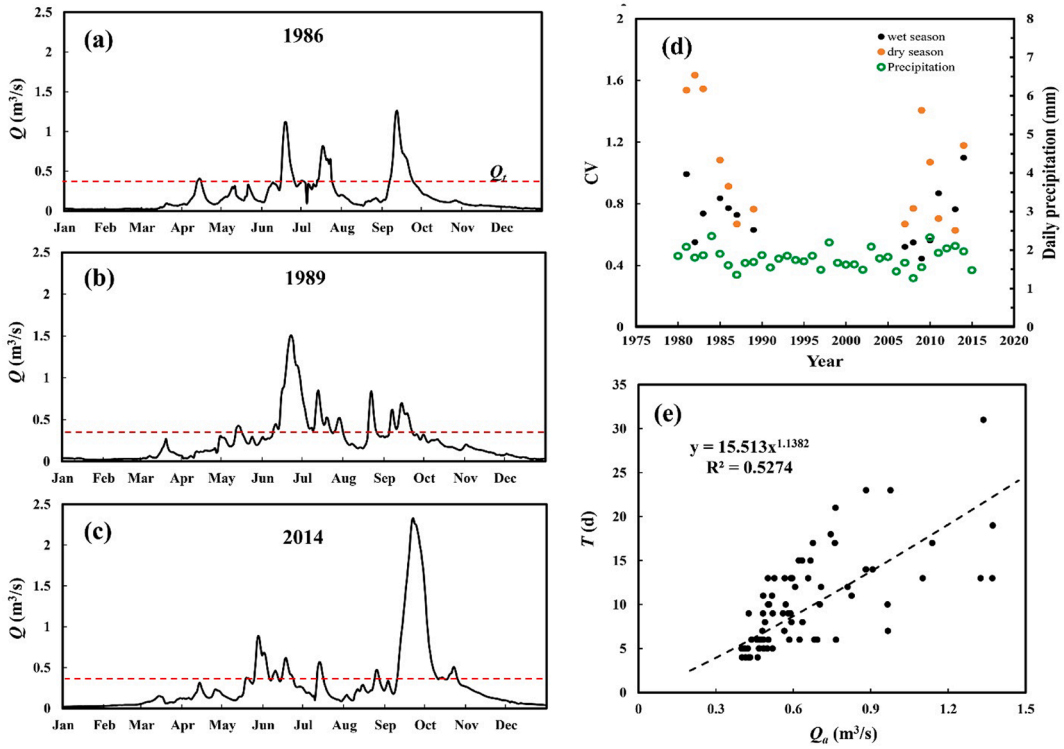

Fig. 3. Characteristics of the obtained daily discharges in 14 discontinuous years at the reference cross section. (a) – (c) Examples of annual daily discharges in 1986, 1989, and 2014; (d) Plot of coefficient of variation (CV) of daily discharges and annual mean daily precipitation vs. years; (e) The relationship between durations of competent hydrographs (T) and the associated mean discharges (Q_a).

(Fig. 3d) showed that Q values in the two separate periods had a similar degree of variation in both seasons. Given that mean annual daily precipitation did not have any obvious temporal trend from 1980 to 2015 (Fig. 3d), it is reasonable to conclude that flow regime has remained similar over the last four decades and the obtained 14-year daily discharges are representative over the entire period. The available above-threshold daily discharges consist of 77 competent hydrographs whose daily discharges can trigger fluvial erosion of the LL, representing about 5–6 erosion events per year on average. The mean daily discharge (Q_a) and the associated time duration (T, days) for the 77 competent hydrographs were significantly correlated with each other (Fig. 3e):

$$T = 15.51 Q_a^{1.138} \quad R^2 = 0.527 p < 0.05 \tag{1}$$

This relationship indicated that (1) the higher the Q_a value, the longer the associated competent hydrograph lasted, and (2) knowing the Q_a value also means that we know the time duration of the associated competent hydrograph. These daily discharges forming 77 competent hydrographs in 14 years were later used to help design theoretical hydrographs for modeling.

2.3.2. Calibration of model parameters

In BSTEM, the magnitude of fluvial erosion (E_f) is determined by (Darby et al., 2007)

$$E_f = k(\tau - \tau_c)\Delta t \tag{2}$$

where k is the erodibility coefficient ($\times 10^{-6}$ m^3 (N − s)$^{-1}$), τ is the shear stress for a given input discharge (Q), τ_c is the critical shear stress, and Δt is the time step each Q lasted. For a given input discharge, $\tau = \rho g R S = \gamma R S$ where γ is the specific weight, R is the hydraulic radius, and S is the local channel bed slope. Although the five sub-layers dividing the bank profile (Fig. 2b) are required by BSTEM, soil properties in the first four sub-layers are similar, while in the lowest one should be different because meandering rivers in the Zoige basin are all perennial rivers (Fig. 1c-1d and 2c-2d), such that a proportion of the bank profile should be always covered by water. Thus, the value of γ in the first four sub-layers was set as 18 kN/m^3, which was obtained from the default value in BSTEM for silt. Because the lowest sub-layer is always submerged, its γ value was adjusted using the submerged soil density, leading to 8.2 kN/m^3. The value of S, which was 0.0036 (m/m), was measured using a total station in the channel segment around the RCS (Fig. 1b). Determination of R needs to know the stage at the bank toe for a given discharge. This value was determined using the Reference Reach Spreadsheet 4.3 created for channel survey management (Mecklenburg, 2006) based on the RCS profile measured in the field. Values of τ_c and k have been empirically calibrated by comparing the modeled bank retreat rates with those measured from satellite images (Daly et al., 2015). Here, they were calibrated separately. Particle size analysis based on several soil samples from banks around the RCS showed that on average $D_{50} = 8.9 \times 10^{-5}$ m, indicating that bank materials are dominated by fine sand and silts. Examining the default values of τ_c provided in BSTEM showed that they led to unrealistic large fluvial erosion for the bank soils. This is not surprising as the associated dimensionless shear stress, θ_c, was around 0.043, which is even smaller than that for particles in gravel-bed rivers. Examining different values and considering suggested values in previous studies (Church, 2006) gave rise to a reasonable one, $\tau_c = 0.088$ Pa, which is equivalent to $\theta_c = 0.06$ and plausible for the soils in the studied river banks. The erodibility coefficient, k is well known related to τ_c by (Arulanandan et al., 1980; Midgley et al., 2012; Rinaldi et al., 2008)

$$k = m\tau_c^e \tag{3}$$

where $e = -0.5$ and m is a coefficient. Previous experimental studies showed that $m = 2 \times 10^{-7}$ m^2/(N$^{-0.5}$ · s) (Hanson and Simon, 1980; Midgley et al., 2012), but BSTEM adopts $m = 1 \times 10^{-7}$ m^2/(N$^{-0.5}$ ·s), which was also used in this study. Using the calibrated τ_c value led to $k = 3.37 \times 10^{-7}$ m^3/(N·s).

Simulating bank collapse (i.e., geotechnical failure) requires knowledge of the soil failure angle, φ of bank face in the LL and cohesive coefficient, c. Existing values of these two parameters have been primarily obtained from laboratory experiments, such as triaxial test and borehole shear test (Daly et al., 2015; Rinaldi et al., 2004; Simon et al., 2011; Zong et al., 2017). However, application of these values to real riverbanks may not be always appropriate (Klavon et al., 2017). Preliminary BSTEM simulation using the default value in BSTEM, $\varphi = 26.6°$, showed that it bank collapse occurred unrealistically fast. Given that $\varphi = 30°$ is the median value used in past modeling analyses (see Fig. 1b in Klavon et al., 2017), it was adopted in this study. For c, the value of 5.5 kPa was indirectly determined with the aid of field data as follow. Measured widths of overhanging arms (W) in 33 existing cantilever banks along the Black River ranged between 0.1 and 0.58 m (Fig. 4). Given that these overhanging arms were at different stages of their development toward cantilever failure, the range of W values, together with our field observation suggested that the threshold width of the overhanging arm (W_c) should be no less than 0.6 m. With this reference, calibration modeling led to the selected value of c. Since the top surface of the model structure is protected by the upper cantilever layer, its c value should be greater than that used in other layers. In this study, it was increased by 20% for the top sub-layer.

2.4. Design of theoretical hydrographs for modeling

The design of theoretical hydrographs for modeling was guided by the converted daily discharges in the Black River at the RCS. Among all 77 competent hydrographs, only those in 1983 were capable of triggering two cantilever failure of the upper (soil-vegetation mixture) layer as the average width of the overhang arm (W) was 1.02 m, much greater than the threshold (i.e., 0.6 m). In six years (1981, 1982, 1985, 1989, 2013, and 2014), such failure only occurred one time and their W values varied between 0.53 and 0.56 m (Table 1). There were five years (1986, 1987, 2009, 2010, and 2011) when cantilever failure of the upper layer did not happen, though 21 competent hydrographs caused some fluvial erosion.

These results indicated that on average cantilever failure (CF) of the entire composite bank happened in about 1–2 years, suggesting that composite bank erosion in the alpine meander rivers of the Zoige basin is controlled by fluvial erosion and bank collapse in the lower layer (LL). Competent hydrographs whose mean discharge (i.e., Q_a) is less than 1.0

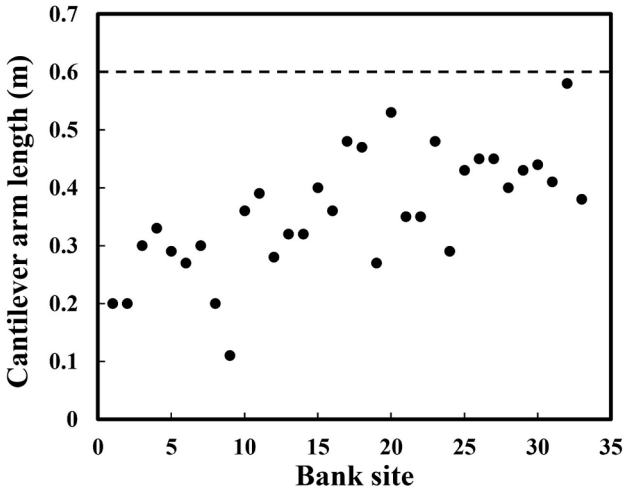

Fig. 4. Widths of overhang arms measured in the Black River within the Zoige basin. They represent cantilever banks developed at different stages. The dashed horizontal line signifies the threshold value initiating cantilever failure of the upper soil-vegetation layer.

Table 1
Simulated cantilever width during one cycle of bank erosion using obtained competent hydrographs in each of the 14 years.

Years	Total number of competent hydrographs	Q_a *(m^3/s)	Q_p **(m^3/s)	Number of cantilever failure	Overhang width (m)
1981	6	0.50–1.37	1.93	1	0.56
1982	11	0.40–1.14	1.67	1	0.56
1983	9	0.41–1.37	1.81	2	1.02
1985	5	0.47–1.05	1.70	1	0.56
1986	3	0.61–0.75	1.26	0	0
1987	6	0.46–0.83	1.28	0	0
1989	9	0.41–0.98	1.51	1	0.56
2007	0	–	0.16	0	0
2008	0	–	0.21	0	0
2009	4	0.40–0.62	0.83	0	0
2010	5	0.48–0.68	0.97	0	0
2011	3	0.50–0.76	1.16	0	0
2013	8	0.41–0.88	1.41	1	0.55
2014	8	0.43–1.34	2.33	1	0.53

* The mean of daily discharges in each competent hydrograph.
** The peak discharge among all daily discharges in the seven competent hydrographs with the same Q_a.

m^3/s, could hardly cause CF, as in only two out of 14 years (1989 and 2013), CF was caused by competent hydrographs with Q_a slightly less than 1.0 m^3/s. Flood frequency analysis using annual maximum discharges (Q_m) showed that in competent hydrographs with $Q_a = 1.0$ m^3/s, Q_m had recurrence interval of greater than two years. Thus, it is clear that emergence of CF is an episodic event comparing with continuous fluvial erosion. The occurrence of CF in Table 1 essentially represents the occurrence of bank collapse simulated using BSTEM in the LL that may lead to the width of overhanging arm (W) equal or greater than $W_c = 0.6$ m. A cycle of bank erosion ends after the occurrence of bank collapse in the LL with $W_c > 0.6$ m because this bank collapse will induce CF of the upper layer and the failed soil-vegetation mixture will cover the bank toe for a relatively long time period. It follows that the case of one competent hydrograph causing two continuous CFs (Table 1) is not realistic and should not be taken into consideration in the subsequent design of competent hydrographs.

Based on these results, five sets of theoretical competent hydrographs were designed to attempt to reflect the full range of erosional processes controlling the cycle of bank erosion. Each set contains seven competent hydrographs whose lowest Q values were greater than $Q_t = 0.373$ m^3/s and that have the same Q_a value, but different shapes. The hydrograph shape is controlled by three parameters, the initial daily discharge (Q_i), the peak daily discharge (Q_p), and the time of occurrence of Q_p, expressed as a percent of the time at which Q_p occurs (T_p) with respect to the entire time of the hydrograph (T). The five sets of designed competent hydrographs had Q_a values of 1.0, 1.2, 1.4, 1.6, and 1.8 m^3/s, respectively (Table 2 and Fig. 5). These competent hydrographs cover not only the range of existing daily discharges (Table 1), but also those have not happened yet (e.g., many daily discharges in $Q_a = 1.6$ and 1.8 m^3/s).

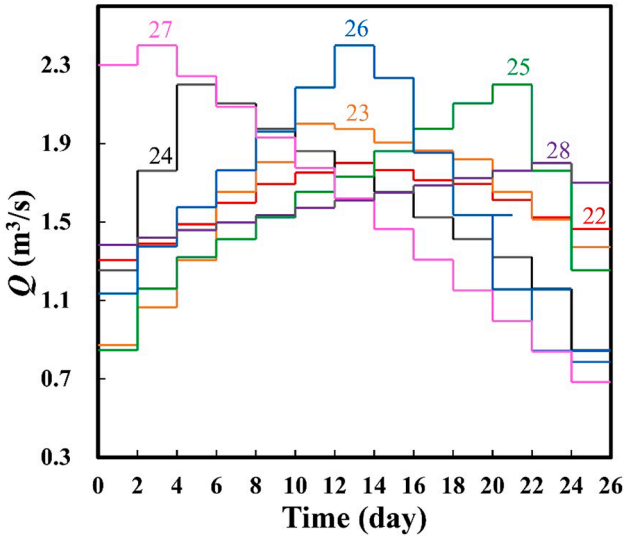

Fig. 5. An example of the variable daily discharges designed as hydrographs with the same mean discharge of 1.6 m^3/s. Each hydrograph had a different shape characterized by a different combination of Q_i, Q_p, and T_p. The numbers on these hydrographs (22–28) are consistent with those in Table 2.

2.5. Analyses of model outcomes

Using these designed competent hydrographs, both fluvial erosion and bank collapse in the LL were simulated (see the full outcomes in the appendix). The former was expressed as the amount of eroded bank materials (E_f, m^3), while the latter was denoted as the volume of failed bank body (E_c, m^3). The modeled E_f and E_c values were examined for exposing the impact of hydrograph shapes on their variability, which was further confirmed by calculating the relative sensitivity (S_r) of Q_i, Q_p, and T_p with respect to changes of E_f. Values of S_r were calculated using the following equation (Cancienne et al., 2008):

$$S_r = \left(\frac{O - O_b}{I - I_b}\right)\left(\frac{I_b}{O_b}\right) \quad (4)$$

where O is output, which refers to E_f in this study, I is input, which denotes Q_i, Q_p, and T_p, respectively, subscript b indicates the baseline value, which was selected here as values at $Q_a = 1.0$ m^3/s.

This analysis provided necessary information for identifying a proportion of the five sets of competent hydrographs that could realistically occur under the existing flow regime of the Black River. The identification relied on comparing the existing 77 competent hydrographs with the designed ones in terms of Q_i values and the $Q_p - Q_a$ relationships. Using these identified realistic competent hydrographs, the relationships between the predicted E_f and E_c and the Q_a values were established to characterize the dominant role of Q_a values in controlling bank erosion, which was followed by determining hydrograph-based effective

Table 2
Characteristics of the designed five sets of hydrographs.

Hydrographnumber	Q_a(m^3/s)	Q_p (m^3/s)	Q_i (m^3/s)	T (d)	T_p	E_{fm} (m^3)	(E_{fmax}-E_{fmin})/E_{fmin}	E_{fv}(%)	E_{cm} (m^3)	(E_{cmax}-E_{cmin})/E_{cmin}	E_{cv} (%)
1–7	1.0	1.2–1.8	0.39–1.70	16	0.25–0.88	0.043	1.733	40.63	0.325 (1)*	/	/
8–14	1.2	1.4–2.0	0.40–1.90	20	0.20–0.90	0.065	1.564	41.06	0.336 (3)*	0.046	2.31
15–21	1.4	1.6–2.2	0.40–2.10	22	0.18–0.91	0.089	1.418	37.59	0.342 (4)*	0.070	3.08
22–28	1.6	1.8–2.4	0.85–2.30	26	0.15–0.92	0.168	1.283	28.95	0.473 (7)*	1.048	36.99
29–35	1.8	2.0–2.6	0.99–2.50	30	0.13–0.93	0.237	0.740	20.29	0.551 (7)*	1.090	38.26

Note: Q_i is the initial daily discharge in each of the designed competent hydrograph, T is the duration of each designed competent hydrograph, and T_p is the time of occurrence of Q_p, expressed as a percent of the time at which Q_p occurs with respect to T. E_{fm} is the mean of the total volume of fluvial erosion, E_{fv} is the coefficient of variation for E_f. E_{cm} and E_{cv}, are the associated variables for bank collapse.
* This number stands for the number of hydrographs within each set that triggered bank collapse.

discharges and revealing their geomorphological significance.

3. Results and analysis

3.1. Impact of shapes of hydrographs on bank erosion

For the first set with Q_a = 1 m^3/s, the relative error of simulated fluvial erosion (E_f), defined as the ratio of the difference between minimum and maximum E_f values (E_{fmin} and E_{fmax}) to E_{fmin}, was 173% (Table 2), meaning the simulated E_f could be about 200% different when the shape of competent hydrographs changed. Except the one producing E_{fmax}, other competent hydrographs led to similar E_f values (Fig. 6a). A similar pattern existed for the results from the seven competent hydrographs with Q_a = 1.4 m^3/s (Fig. 6a). These E_f values generated a lower range of difference (141%) (Table 2). Competent hydrographs with Q_a = 1.2 m^3/s resulted in E_f values that may be separated into two different clusters (Fig. 6a) and may create possible errors up to 156% (Table 2). The two sets of competent hydrographs with Q_a = 1.6 and 1.8 m^3/s could create less degrees of errors among (128% and 74%, respectively), but the simulated E_f values were more dispersed (Fig. 6a). These results indicated that for competent hydrographs with the same Q_a value, differences in their shapes could cause significant difference in the simulated E_f values, such that use of their mean value (i.e., E_{fm}) would cause discernable errors for some competent hydrographs with the same Q_a value (Fig. 6a). The coefficient of variation (i.e., E_{fv}) decreased with the increase of Q_a values, indicating that the degree of variation among these E_f values was higher for competent hydrographs with less Q_a values (Table 2).

Simulated bank collapse (E_c) demonstrated a more complex situation. Only in those with Q_a = 1.6 and 1.8 m^3/s could all competent hydrographs trigger bank collapse (Table 2). For the three sets with smaller Q_a values, there were only one, three, and four competent hydrographs that triggered bank collapse (Table 2). Accordingly, the impact of variable competent hydrographs on E_c was reflected in both magnitude and frequency of E_c. For those with Q_a = 1.6 and 1.8 m^3/s, differences among competent hydrographs in each set could cause over 100% differences in E_c, making their means (i.e., E_{cm}) considerably different from actual higher or lower values (Fig. 6b and Table 2). At relatively low Q_a values (1.2 and 1.4 m^3/s), E_c values caused by some competent hydrographs were similar with much smaller coefficient of variation (i.e., E_{cv}) than those from competent hydrographs with higher Q_a values (Table 2). Therefore, the impact of variable competent hydrographs on E_c values was more significant at higher Q_a values. On the other hand, at lower Q_a values, many competent hydrographs were incapable of initiating bank collapse. At Q_a = 1.0 m^3/s, only about 14% of competent hydrographs with variable shapes may trigger bank collapse, while at Q_a = 1.4 m^3/s, this probability was increased to about 57% (Fig. 6c). For competent hydrographs with $Q_a \leq$ 1.6 m^3/s, this probability was highly correlated with Q_a:

$$P = 16.3Q_a^{3.95}\ R^2 = 0.956 p < 0.05 \quad (5)$$

where P is the probability of competent hydrographs with the same Q_a value that may trigger bank collapse. The strong correlation between P

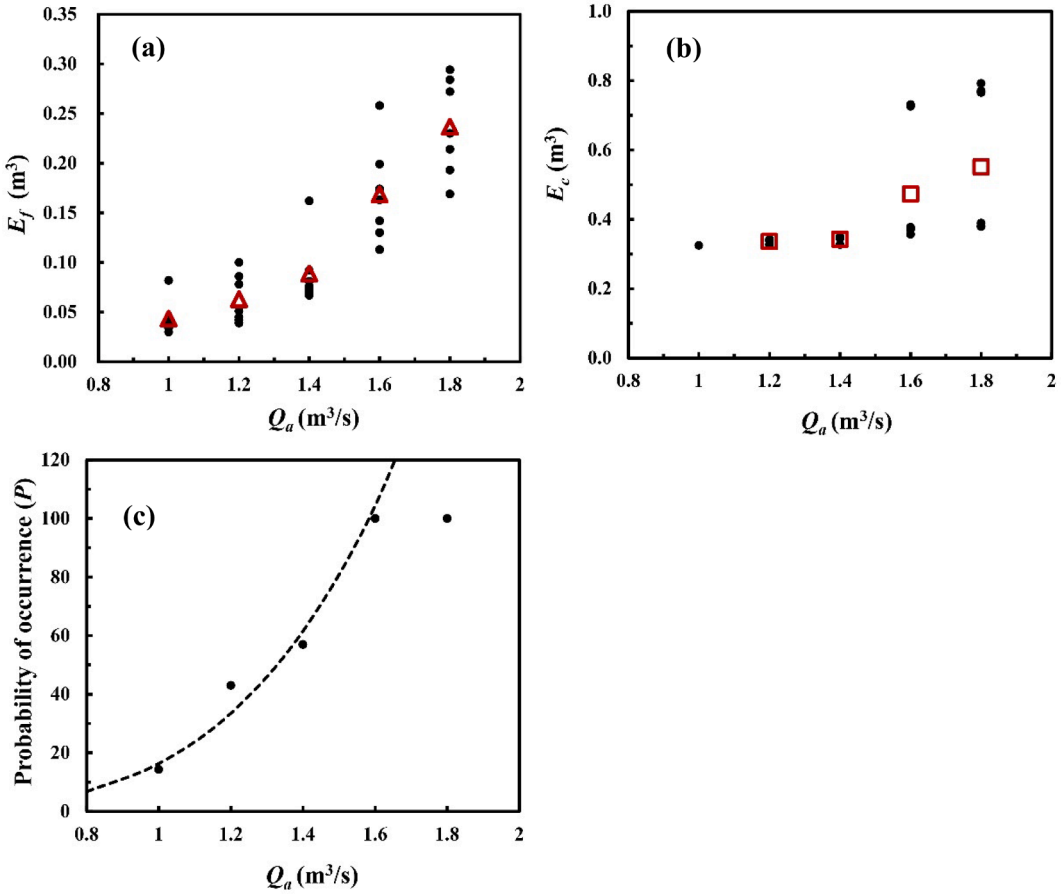

Fig. 6. Modeled results for fluvial erosion (E_f) and bank collapse (E_c) under five sets of competent hydrographs with the same mean discharges. (a) Variable values of E_f caused by these competent hydrographs. The red triangles represent the means of E_f values for each set of competent hydrographs; (b) Variable values of E_c caused by these competent hydrographs. The red rectangles represent the means of E_c values for the sets of competent hydrographs that may trigger bank collapse; (c) Probability of occurrence for bank collapse caused by competent hydrographs with the same mean discharges. The fitted dashed curve represents Eq. (5). (For interpretation of the references to colour in this figure legend, the reader is referred to the web version of this article.)

and Q_a indicated that for a given Q_a value lower than 1.6 m^3/s, not all competent hydrographs are able to trigger bank collapse and the lower the Q_a value is, the lower probability of competent hydrographs that may cause bank collapse is. Below $Q_a = 1.6$ m^3/s, different shapes of competent hydrographs with the same Q_a values mainly affect the frequency of occurrence for bank collapse because once occurred, E_c values tended to be similar (Fig. 6b and 6c). Above this threshold, shape variations of competent hydrographs primarily influence the magnitude of E_c.

Although variations of competent hydrographs with the same Q_a values would lead to significantly different amounts of E_f and E_c, their impacts on E_f are only reflected by variable magnitudes of E_f, whereas on E_c are denoted by both variable and episodic values of E_c. Therefore, further examination of how shapes of competent hydrographs affect bank erosion was achieved by analyzing sensitivity of the three parameters, Q_i, Q_p, and T_p to modeled E_f values. The analysis showed that the mean relative sensitivity (S_r) for Q_i, Q_p, and T_p was 1.7, 1.4, and −0.2, respectively. These S_r values suggested that Q_i is most sensitive to the predicted E_f values. A higher variation in Q_i value would cause a higher degree of variation in the predicted E_f values. It is interesting to note that variation in Q_p is not the most dominant factor that leads to variations in E_f values as in the case of sediment transport (Duvert et al., 2012; Hicks, 1994; Hicks et al., 2004).

3.2. Identification of the realistic competent hydrographs

As mentioned above, not all theoretically designed competent hydrographs have happened in reality. Therefore, identification of possibly realistic competent hydrographs may be based on characteristics of the actual competent hydrographs described previously. Calculation using the 77 competent hydrographs showed that about 87% of Q_i values tended to be in the range between 0.373 and 0.6 m^3/s (Fig. 7a), suggesting that competent hydrographs with very high Q_i values (>1.0 m^3/s) might be very rare in reality. Further analysis signified that Q_p values were very closely related to Q_a values (Fig. 7b):

$$Q_p = 1.438Q_a^{1.274} \quad R^2 = 0.944 p < 0.05 \tag{6}$$

As Q_a increased, the associated Q_p became more scattered around Eq. (6), indicating that higher degrees of uncertainties exist in possible realistic Q_p values for competent hydrographs with higher Q_a values. However, even considering these high degrees of uncertainties, competent hydrographs represented by the three lower red points for Q_a = 1.6 and 1.8 m^3/s were less likely to occur (Fig. 7b), because their existence would change Eq. (6), which was based on the true competent hydrographs. At $Q_a = 1.4$ m^3/s, competent hydrographs represented by the lowest red point were not realistic, while at Q_a = 1.2 m^3/s, competent hydrographs reflected by the lowest and highest red points were not realistic for the same reason. Among the last set of competent hydrographs with $Q_a = 1.0$ m^3/s, those associated with the highest point were not realistic because they had unrealistically high Q_i values. The selected competent hydrographs were more realistic and used for further analysis.

3.3. Hydrograph-based erosion rating curves

Examining these realistic competent hydrographs and their predictions indicated that both E_f and E_c were strongly correlated with the Q_a values of these competent hydrographs (Fig. 8):

$$E_f = 0.034Q_a^{2.905} \quad R^2 = 0.878 p < 0.05 \tag{7a}$$

$$E_f = 0.313Q_a^{0.313} \quad R^2 = 0.625 p < 0.05 \tag{7b}$$

Both Eqs. (7a) and (7b) indicated that variations of E_f and E_c may be sufficiently controlled by Q_a values of competent hydrographs regardless of their shapes. The implication is that though variations in shapes

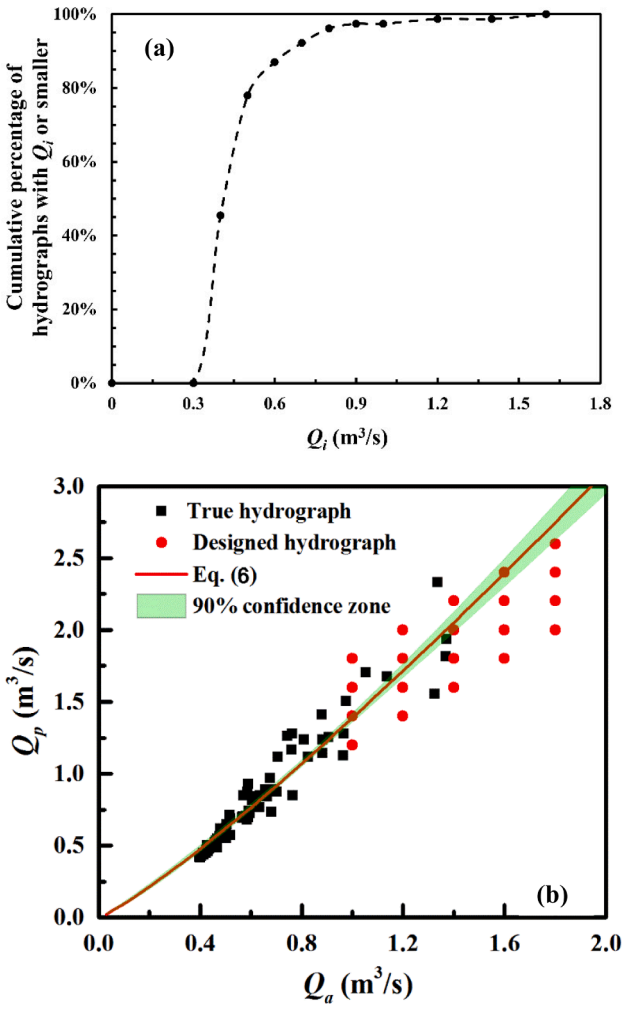

Fig. 7. Characteristics of the 77 obtained and the five sets of designed competent hydrographs. (a) Cumulative percentages of the obtained competent hydrographs having the value lower or equal to each of the given Q_i values; (b) The relationship between Q_p and Q_a. The solid red line represented Eq. (6) developed based on the obtained competent hydrographs. The 90% confidence zone was marked for assisting the selection of the realistic competent hydrographs from the designed ones. For each designed Q_a value, there were actually seven competent hydrographs, some of which had the same Q_p values. (For interpretation of the references to colour in this figure legend, the reader is referred to the web version of this article.)

of competent hydrographs with the same Q_a value may cause variable amounts of predicted E_f and E_c, this impact is secondary compared with that of competent hydrographs with different Q_a values. Therefore, the impact of variable discharges arranged as competent hydrographs on both fluvial erosion and bank collapse is largely controlled by the Q_a values of these hydrographs. Following this line, Eq. (7a) can be viewed as a hydrograph-based rating curve for determining amounts of E_f caused by individual competent hydrographs. Although Eq. (7b) may be viewed in the same way for E_c, the predicted E_c value using Eq. (7b) for a given Q_a may not occur in reality, because the probability of this occurrence is controlled by Eq. (5) (Fig. 6c). Therefore, the hydrograph-based erosion rating curve for E_c should consider both Eq. (7b) as magnitude and Eq. (5) as frequency.

3.4. Hydrograph-based effective discharges

The hydrograph-based rating curves for E_f and E_c make it possible to determine the most effective competent hydrograph that shapes riverbanks, if an appropriate flow duration curve for competent hydrographs

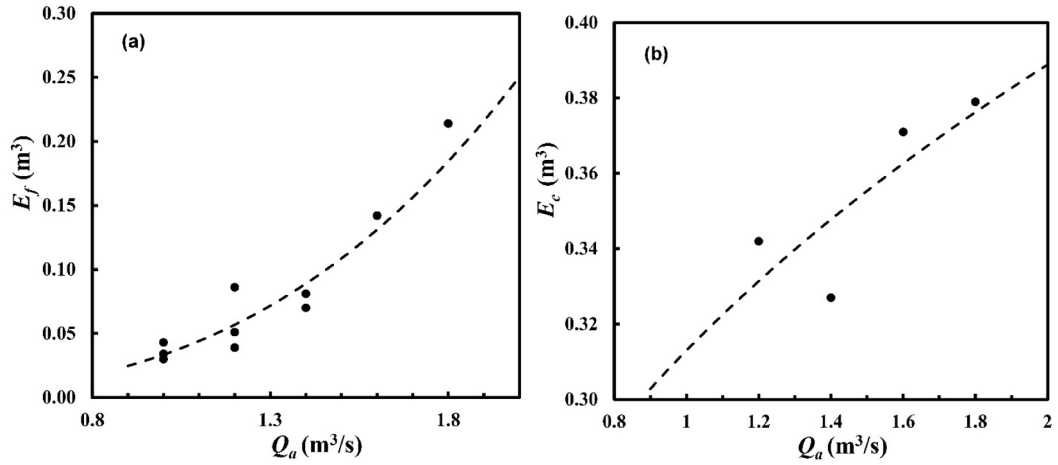

Fig. 8. The hydrograph-based effective discharges (Q_e) for (a) fluvial erosion (E_f) and (b) bank collapse (E_c). The dashed curves represent Eqs. (7a) and (7b).

may be established. Within the obtained series of daily discharges over the 14 years, those constituting competent hydrographs can be represented by a new series of Q_a. Since each Q_a implies a time duration (T) of the associated competent hydrograph (Fig. 2e), the series of Q_a includes the magnitude of Q_a and the associated T. Thus, using the identified 77 competent hydrographs in the 14 years, we were able to develop a hydrograph-based flow duration curve (FDC) (Fig. 9a):

$$P_d = 4.062e^{-3.30Q_a} \; R^2 = 0.994 p < 0.05 \tag{8}$$

where P_d is the probability of time a given discharge is equaled or exceeded. Eq. (8) is different from the classic FDC based on continuous daily discharges over the same 14 years (Fig. 9a). The cumulative probability of each Q_a was calculated using the total period of the 77

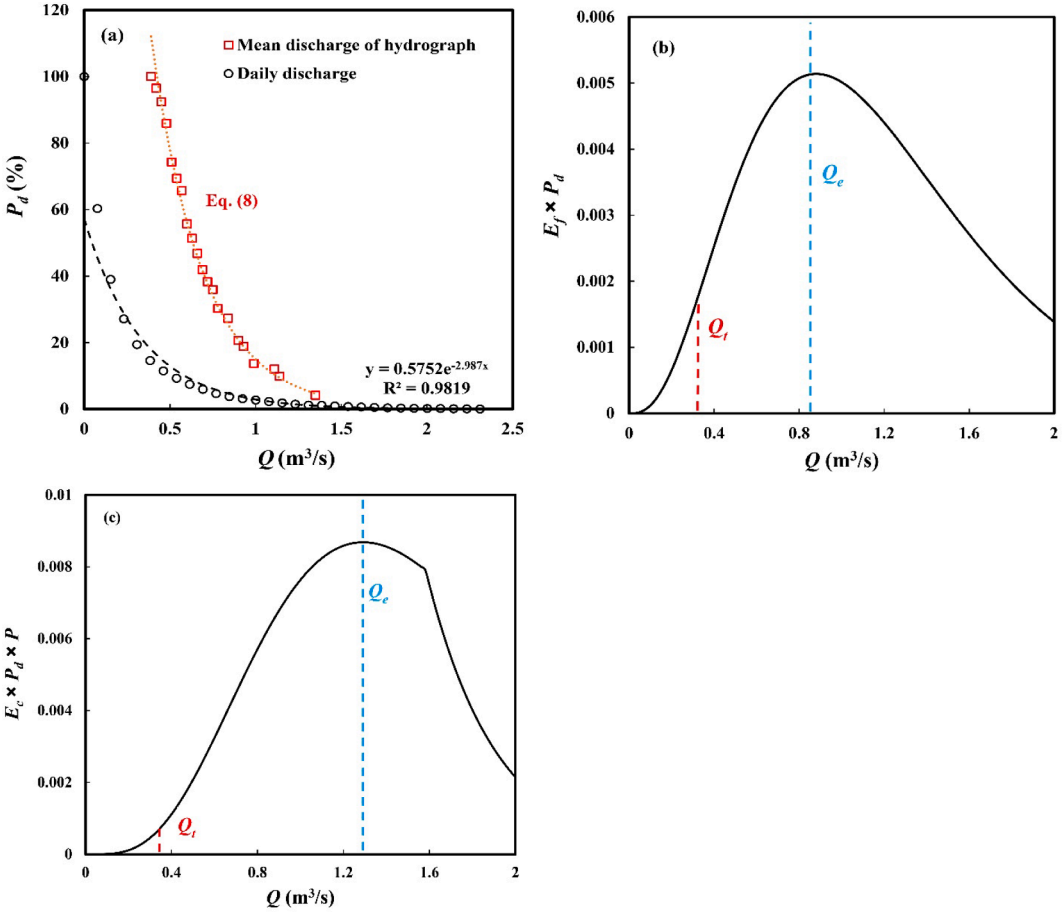

Fig. 9. The hydrograph-based effective discharges for fluvial erosion (E_f) and bank collapse (E_c). (a) Flow duration curves based on the mean discharges of all competent hydrographs (red) and the daily discharges (dark). P_d is the probability of time a given discharge is equaled or exceeded; (b) The effective discharge (Q_e) for E_f, which is 0.880 m^3/s. Q_t denotes the threshold discharge that can initiate fluvial erosion; (c) The effective discharge (Q_e) for E_c, which is 1.292 m^3/s. P is the probability of occurrence of bank collapse illustrated in Fig. 6. (For interpretation of the references to colour in this figure legend, the reader is referred to the web version of this article.)

competent hydrographs, which was 774 days, rather than the entire period of 14 years, which was 5111 days. Thus, statistically, these probabilities are similar to the concept of conditional probability with regard to the classic probabilities for daily discharges. Hydrologically, a given Q_a with a magnitude the same as that of the daily discharge would result in a higher exceeding probability, but as the magnitude increases, the difference between the two exceeding probabilities becomes smaller (Fig. 9a). Essentially, flow regime based on variable daily discharges arranged in hydrographs is more flashy than that of the original daily discharges. In other words, a small increase of Q as the mean discharge of competent hydrographs would cause a greater degree of decrease in exceeding probability than that of Q as the daily discharge would do.

Following its definition, the effective discharge (Q_e) for fluvial erosion of the LL may be determined from the product of Eqs. (7a) and (8), while that for bank collapse of the LL could be calculated from the product of Eqs. (5), (7b), and (8). The identified Q_e for E_f and E_c was 0.880 and 1.292 m^3/s, respectively (Fig. 9b and 9c). This value represents the effect of a group of variable discharges forming a competent hydrograph on bank erosion and thus is denoted as the hydrograph-based effective discharge. For fluvial erosion, The Q_e = 0.880 m^3/s was greater than the threshold value (Q_t = 0.373 m^3/s), suggesting that any competent hydrograph with this Q_e value can most effectively remove bank materials in the LL (Fig. 9b), though possible variations in the shape of competent hydrograph may shift the magnitude of fluvial erosion slightly. It characterizes the collective effect of a series of variable daily discharges whose mean equals Q_e on fluvial erosion. For bank collapse, Q_e = 1.292 m^3/s was greater than not only Q_t, but also Q_e for fluvial erosion, signifying that competent hydrographs with a higher Q_a value can most effectively cause bank collapse (Fig. 9c). Overall, these results showed that the progressive fluvial erosion and episodic bank collapse are dominated by variable daily discharges arranged in competent hydrographs, the former requires competent hydrographs with a lower Q_a value than the latter does.

4. Discussion

4.1. Nature of our modeling and potential limitations

It should be noted that the conceptual model introduced in this study is different from the classic one that treats the lower layer (LL) and the upper mixed layer as an integrated bank profile (Daly et al., 2015, 2007; Patsinghasanee et al., 2018; Rousseau et al., 2017). Thus, when BSTEM was applied to the classic model, an implicit assumption is that the LL is only subject to fluvial erosion. In the Black River within the Zoige basin, there are many discernable cases in which retreat of LL could be caused by bank collapse. These cases support the idea of allowing the LL to be shaped by both fluvial erosion and bank collapse.

Quality of BSTEM modeling relies on accuracy of input discharges and model key parameters. Although there are 77 competent hydrographs in the available true daily discharges, they were not used in developing competent effective discharges because these hydrographs do not include realistic, but not yet occurred high-magnitude hydrographs (e.g., those with Q_a = 1.6 and 1.8 m^3/s, see Fig. 7b), which are capable of triggering bank collapse. Nonetheless, modeling results using these competent hydrographs (Table 1) provided valuable references for designing the theoretical competent hydrographs. It is admittable that selection of the key model parameters involved certain uncertainties. In particular, selection of the c value on the top sub-layer (Fig. 2b) was subjective. To test its reliability, we performed, using the input hydrograph 22 and 26 (Table 2 and Fig. 5), sensitivity analysis by comparing E_f and E_c values based on the selected c value with those in terms of other c values. For hydrograph 22, changes of the c value by no more than 20% would lead to at most 13% overestimation of E_f and no changes in E_c (Fig. 10a). Continuous increase of the c value by 30–40% would cause E_f to be underestimated from 5% to 18% and E_c to be underestimated by about 18%. For hydrograph 26, however, increase of the c value up to 40% would not cause any discernable changes in E_f and E_c values (Fig. 10b). These results showed that increasing the c value by different percentages (rather than 20% as did in our modeling) would cause limited variations in the modeled E_f and E_c values. It appeared that our choice was reasonable.

Despite of possible uncertainties still existing in other key parameters, including ignorance of possible freeze-thaw impact on bank erosion at later stages, the purpose of modeling is not for accurately predicting bank retreat rates, but for revealing hidden geomorphological characteristics in the processes of bank erosion. Therefore, the fact that selected values of the key parameters allowed for reasonable prediction of bank retreat rates caused by annual competent hydrographs (Table 1), suggested that the modeling appropriately captured hydrodynamic processes of composite bank erosion in the meandering rivers within the Zoige basin.

4.2. Geomorphological significance of discharge variability

Findings in this study indicated that processes of composite bank erosion in the prototype rivers of the Zoige basin are essentially controlled by variable daily discharges arranged in competent hydrographs, which are characterized by their shapes and mean discharges (Q_a). Among the three shape parameters, the initial discharge (Q_i) and the peak discharge (Q_p) are more sensitive to the impact of the hydrograph shape on bank erosion and their changes may be effectively reflected by coefficient of variation (CV) of a competent hydrograph. Therefore, the geomorphological role of the shape of a competent hydrograph in affecting bank erosion may be revealed by examining the RI - Q_a and CV - Q_a relationships (Fig. 11) where RI is the recurrence interval of the highest possible Q_p in all possible hydrographs with the

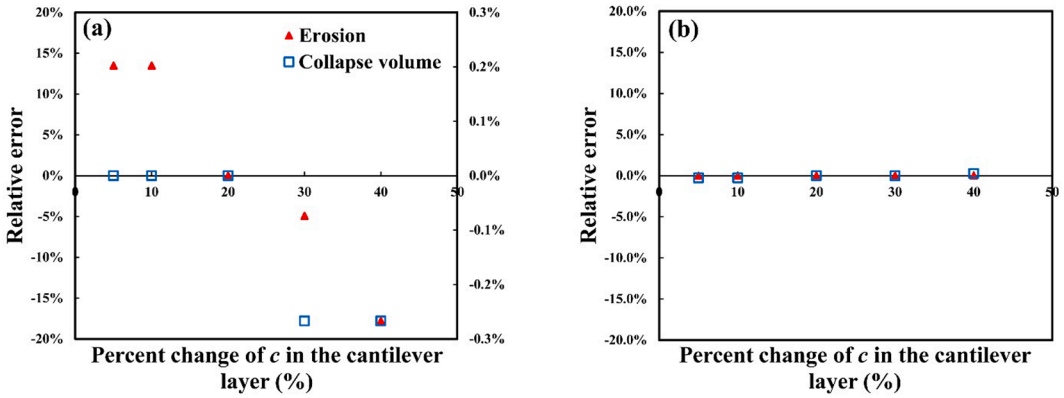

Fig. 10. Sensitivity analysis on the selection of cohesive coefficient, c at the top sub-layer of the conceptual model structure using two competent hydrographs as input daily discharges. (a) Results based on hydrograph 22; (b) results based on hydrograph 26.

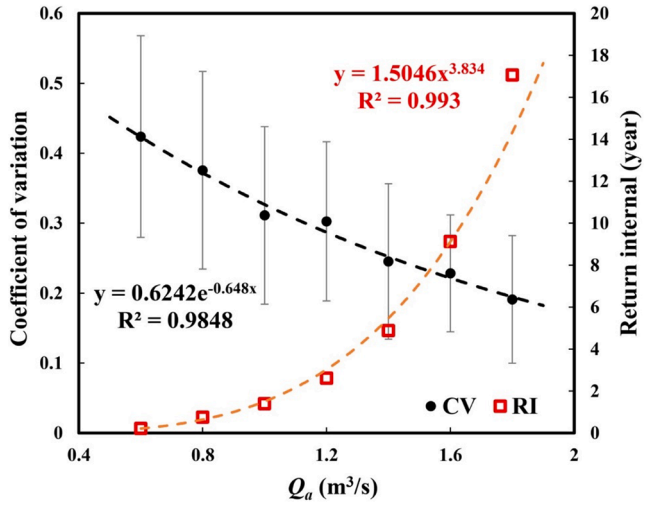

Fig. 11. Two different relationships based on the 77 obtained competent hydrographs, $CV - Q_a$ and $RI - Q_a$ where CV is the coefficient of variation of a competent hydrograph and RI is the recurrence interval of the maximum peak discharges among seven competent hydrographs in each set.

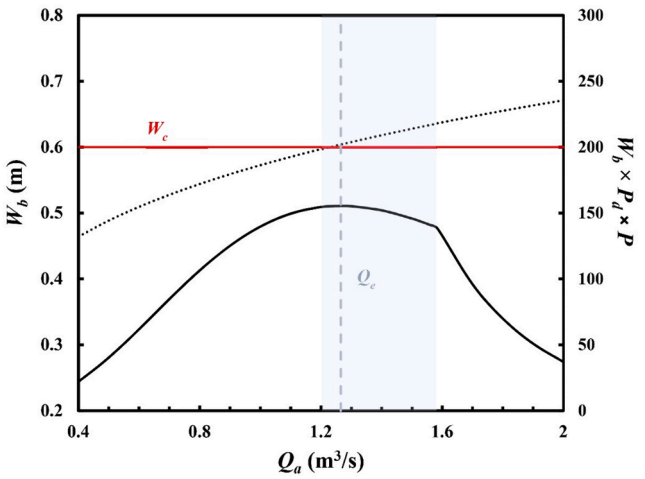

Fig. 12. The hydrograph-based effective discharge for the width of the overhanging arm (W_b), Q_e = 1.265 m^3/s. W_c is the threshold width at which cantilever failure occurs. The dashed curve denotes the hydrograph-based rating curve for W_b, developed as the product of Eqs. (7b) and (9). The shaded range refers to the Q_a values whose associated competent hydrographs are capable of triggering cantilever failure.

same Q_a. As Q_a increases, RI increases, but the degree of the variation of the discharges (i.e., CV) in these competent hydrographs surprisingly decreases. This decrease is at odds with the increased difference between Q_p and Q_t, which defines the traditional concept of sluggish and flashy flow regimes (Bierman and Montgomery, 2014). The two different trends reveal a coupled mechanism of negative feedback on the balance between magnitude and frequency of processes controlling composite bank erosion: while a higher Q_p leads to a larger RI, meaning the associated event/hydrograph becomes rare, it also causes reduction of discharge variability (Fig. 11), better facilitating composite bank erosion owing to more concentrated discharges. Thus, the shape of a competent hydrograph affects processes of bank erosion by determining how discharges within a competent hydrograph are clustered.

Nonetheless, the shape impact of competent hydrographs on the processes of bank erosion is secondary to that of the Q_a values of competent hydrographs, which may be quantitatively determined using our proposed hydrograph-based effective discharge (Q_e). Different from the earlier modification of the classic concept that was based on the total sediment load over a group of discrete discharges (Doyle and Shields, 2008), this concept reflects the lumped effect of variable competent daily discharges on bank erosion. Yet, different Q_e values have to be used to quantify processes of fluvial erosion and bank collapse (Fig. 9b and 9c) because of their different nature (i.e., progressive versus episodic). This difference in Q_e values constrains the ability of this new concept (i.e., the hydrograph-based effective discharge) in revealing dominant processes of controlling bank erosion and broadly river evolution. To overcome this dilemma, the focus may be changed to morphological response of river banks to these two distinct processes. Specifically, the investigation may be switched to bank retreat as the consequence of both fluvial erosion and bank collapse in the LL, which may be quantified using the width of the overhanging arm due to bank collapse of the LL (W_b). The above-mentioned modeling analysis allowed for linking W_b to E_c by the following equation:

$$W_b = 1.340E_c^{0.732}\ R^2 = 0.884 p < 0.05 \quad (9)$$

Combining Eq. (9) with Eq. (7b) readily led to a relationship between W_b and Q_a that may be termed as the hydrograph-based rating curve for W_b. Since the occurrence of W_b is also determined by the two probabilities (i.e., Eqs. (5) and (8)), the hydrograph-based effective discharge for W_b can be identified as $Q_e = 1.265\ m^3/s$ (Fig. 12). Once a hydrograph with $Q_a = Q_e$ triggers bank collapse of the LL, it will create an overhanging arm with the width (W_b) greater than W_c. Thus, cantilever failure will occur and a cycle of bank erosion will be completed. The shape of the curve representing $W_b \times P_d \times P$ indicted that competent hydrographs with Q_a values ranging between 1.2 and 1.585 m^3/s are all effective in generating an overhanging arm (i.e., the shaded range in Fig. 12). Furthermore, once an overhanging arm is created by a competent hydrograph with Q_a values in this range, it always triggers cantilever failure as $W_b \geq W_c$. Given that competent hydrographs with Q_a values falling in this range merely occur in<15% of the 14-year period (Fig. 9a) and completion of a cycle of bank erosion will cease the process of bank erosion for a while, bank retreat rate should be very low in the prototype rivers of the Zoige basin. It follows that lateral migration rates of meandering rivers in this basin are generally low, which explains generally high sinuosity of these meandering rivers in the long-term evolution.

Use of historical satellite images over past three decades allowed for calculating the average bend migration rate of the main downstream channel of the Black River, which led to the result that the annual migration rate is about 1.2 m/yr (unpublished). Converting this rate to the channels in the upstream Black River assuming their difference may be proportionally scaled by their channel widths (Fig. 1), a rate of about 0.2 m/yr may be obtained. This means that cantilever failure occurs on average in a period of more than one year, which is consistent with the fact that competent hydrographs with $Q_a \geq 1.2\ m^3/s$ tend to emerge at least every two years or more (based on flood frequency analysis). The Zoige basin belongs to the Qinghai-Tibet plateau that has been subject to continuous climate warming, which has intensified glacier and permafrost melt (Kang et al., 2010; Li et al., 2020; Yao et al., 2012) and subsequently affected the current hydrological regime. The proposed hydrograph-based effective discharge in this study may serve as a tool to quantify this effect if measurement of daily discharges continues.

In a broader sense, the success of using this new concept in explaining the complex processes of composite bank erosion demonstrates the advantage of characterizing variable discharges in the form of hydrographs for understanding complex and confusing fluvial processes. For instance, whether a given storm event in a river may swipe channel width is not controlled by its peak discharge (i.e., Q_p), but the mean (i.e., Q_a). If $Q_a \geq Q_e > Q_t$, then the associated hydrograph has less degree of discharge variability and would more efficiently widen the channel, leading to the cases in some reported rivers (Fryirs et al., 2015; Meyer, 2001; Phillips, 2002; Thompson and Croke, 2013). If, however, $Q_t < Q_a < Q_e$, then the hydrograph has higher discharge variability and would

affect the channel width less effectively, as in other reported rivers (Gardner, 1977; Magilligan et al., 2015; Roy and Sinha, 2014). Use of Q_e reveals the essential role of discharge variability in understanding the dominant effect of a storm event on channel width. In a more general sense, the hydrograph-based effective discharge also provides a new approach that efficiently incorporates the variability of discharges into an easily determined single magnitude to quantify effective flows sculpting natural rivers for managing climate-driven increase of floods both at present and in the future.

5. Conclusions

Fluvial processes controlling composite bank erosion in the Zoige basin, China were examined as an example to explore the roles of variable daily discharges in controlling these processes and whether these roles may be quantified using the classic concept of the effective discharge. Based on the conceptualized composite bank profile constructed using field measurement and observation from the prototype of the real meandering rivers, simulating, using BSTEM, fluvial processes controlling erosion of the lower bank layer was performed based on five sets of theoretical competent hydrographs that were selected based on properties of 77 observed competent hydrographs. The modeling results were subsequently used to analyze changes of magnitude and frequency of fluvial erosion (E_f) and bank collapse (E_c), led to the following conclusions:

(1) Roles of variable discharges in controlling E_f and E_c can be sufficiently quantified by competent hydrographs that may be characterized by their shapes and mean discharges (Q_a). Variation in the shape of competent hydrographs with the same Q_a value, which is quantified by different combinations of three shape parameters, the initial discharge, the peak discharge, and the time of its occurrence, could cause obvious differences in magnitudes of E_f and E_c. The shape variations in competent hydrographs with different Q_a values also create different probabilities of occurrence of E_c. As Q_a increases, variability of competent hydrographs with the same Q_a becomes lower to create a cluster of higher discharges for more efficiently shaping river banks. Therefore, impact of competent hydrographs with the same Q_a, but different shapes on E_f and E_c should not be ignored.

(2) However, Q_a values of competent hydrographs play a dominant role in controlling E_f and E_c. Consequently, there exist hydrograph-based rating curves for E_f and E_c. Using flow duration curve based on Q_a, (Fig. 9a) enabled us to develop a new concept, a hydrograph-based effective discharge (Q_e) for E_f and E_c. The different Q_e value for E_f and E_c reflects the progressive nature of the former, while the episodic character of the latter.

(3) Viewing the processes of composite bank erosion from the perspective of morphological response to these processes, a single hydrograph-based effective discharge for the width of the overhanging arm (W_b) may be further developed. Comparing the pattern of W_b variation with the threshold width for triggering cantilever failure revealed that the rate of cantilever failure is generally low, which serves as a mechanism of explaining the fact that meandering rivers in the study area of dense grass or peat cover are highly sinuous. Thus, the hydrograph-based effective discharge may be a powerful concept and tool for understanding complex processes of fluvial systems in other regions.

Declaration of Competing Interest

The authors declare that they have no known competing financial interests or personal relationships that could have appeared to influence the work reported in this paper.

Acknowledgement

This study was supported by the National Natural Science Foundation of China (51979012, 91647204) and Natural Science Foundation of Hubei Province of China (2020CFB554). The software, BSTEM, was obtained from USDA website: https://www.ars.usda.gov/southeast-area/oxford-ms/national-sedimentation-laboratory/watershed-physical-processes-research/research/bstem/. We thank the Editor (Dylan Ward), E. A. Keller and two anonymous reviewers who provided constructive comments and suggestions that help improve the quality of the paper.

Appendix A. Supplementary data

Supplementary data to this article can be found online at https://doi.org/10.1016/j.catena.2021.105384.

References

Allan, R.P., Soden, B.J., 2008. Atmospheric warming and the amplification of precipitation extremes. Science 321, 1481–1484.
Apurv, T., Mehrotra, R., Sharma, A., Goyal, M.K., Dutta, S., 2015. Impact of climate change on floods in the Brahmaputra basin using CMIP5 decadal predictions. J. Hydrol. 527, 281–291.
Arulanandan, K., Gillogley, E., Tully, R., 1980. Development of a quantitative method to predict critical shear stress and rate of erosion of natural undisturbed cohesive soils. Clin. Exp. Immunol. 3, 305–312.
Baker, V.R., 1977. Stream-channel respoinse to floods, with examples from Central Texas. Geol. Soc. Amer. Bull. 88, 1057–1071.
Biedenharn, D.S., Copeland, R.R., Thorne, C.R., Soar, P.J., Hey, R.D., Watson, C.C., 2000. Effective Discharge Calculation: A Practical Guide. U.S. Army Corps of Engineering, Coastal and Hydraulics Laboratory Report ERDC/CHL TR-00-15, Washington DC.
Bierman, P.R., Montgomery, D.R., 2014. Key concepts in Geomorphology. W.H Freeman and Company Publishers, New Yrok, USA.
Brown, R.A., Pasternack, G.B., 2014. Hydrologic and topographic variability modulate channel change in mountain rivers. J. Hydrol. 510, 551–564.
Cancienne, R.M., Fox, G.A., Simon, A., 2008. Influence of seepage undercutting on the stability of root-reinforced streambanks. Earth Surf. Process. Landf. 33, 1769–1786.
Chen, D., Duan, J.G., 2008. Case study: two-dimensional model simulation of channel migration processes in West Jordan River, Utah. J. Hydraul. Eng. 134, 315–327.
Chen, Y.N., Collins, M.B., Thompson, C.E.L., 2011. Creek enlargement in a low-energy degrading saltmarsh in southern England. Earth Surf. Process. Landf. 36, 767–778.
Church, M., 2006. Bed material transport and the morphology of alluvial river channels. Ann. Rev. Earth Planet. Sci. 34, 325–354.
Crowder, D.W., Knapp, H.V., 2005. Effective discharge recurrence intervals of Illinois streams. Geomorphology 64, 167–184.
Daly, E.R., Miller, R.B., Fox, G.A., 2015. Modeling streambank erosion and failure along protected and unprotected composite streambanks. Adv. Water Resour. 81, 114–127.
Dapporto, S., Rinaldi, M., Casagli, N., Vannocci, P., 2003. Mechanisms of riverbank failure along the Arno River, central Italy. Earth Surf. Process. Landf. 28, 1303–1323.
Darby, S.E., Rinaldi, M., Dapporto, S., 2007. Coupled simulations of fluvial erosion and mass wasting for cohesive river banks. J. Geophys. Res. Earth Surf. 112, F03022. https://doi.org/10.1029/2006JF000722.
Downs, P.W., Soar, P.J., Taylor, A., 2016. The anatomy of effective discharge: the dynamics of coarse sediment transport revealed using continuous bedload monitoring in a gravel-bed river during a very wet year. Earth Surf. Process. Landf. 41, 147–161.
Doyle, M.W., Shields, C.A., 2008. An alternative measure of discharge effectiveness. Earth Surf. Process. Landf. 33, 308–316.
Doyle, M.W., Stanley, E.H., Strayer, D.L., Jacobson, R.B., Schmidt, J.C., 2005. Effective discharge analysis of ecological processes in streams. Water Resour. Res. 41, W11411. https://doi.org/10.1029/2005WR004222.
Duvert, C., et al., 2012. Towards prediction of suspended sediment yield from peak discharge in small erodible mountainous catchments (0.45-22 km(2)) of France, Mexico and Spain. J. Hydrol. 454, 42–55.
Eke, E., Parker, G., Shimizu, Y., 2014. Numerical modeling of erosional and depositional bank processes in migrating river bends with self-formed width: Morphodynamics of bar push and bank pull. J. Geophys. Res. Earth Surf. 119, 1455–1483.
Esposito, C.R., Di Leonardo, D., Harlan, M., Straub, K.M., 2018. Sediment storage partitioning in alluvial stratigraphy: The influence of discharge variability. J. Sediment. Res. 88, 717–726.
Ferrel, K.R.A., Patsinghasanee, S., Kimura, I., Shimizu, Y., 2018. Coupled Model of Bank Erosion and Meander Evolution for Cohesive Riverbanks. Geosciences 8 (10), 359.
Ferro, V., Porto, P., 2012. Identifying a dominant discharge for natural rivers in southern Italy. Geomorphology 139–140, 313–321.
Fryirs, K., Lisenby, P., Croke, J., 2015. Morphological and historical resilience to catastrophic flooding: The case of Lockyer Creek, SE Queensland, Australia. Geomorphology 241, 55–71.

Gao, P., Pasternack, G.B., Bali, K.M., Wallender, W.W., 2008. Estimating suspended sediment concentration using turbidity in an irrigation-dominated southeastern California watershed. J. Irrig. Drain. Eng. 134, 250–259.
Gardner, J.S., 1977. Some geomorphic effects of a catastrophic flood on the Grand River, Ontario. Can. J. Earth Sci. 14, 2294–2300.
Giorgi, F., Raffaele, F., Coppola, E., 2019. The response of precipitation characteristics to global warming from climate projections. Earth Sys. Dynam. 10, 73–89.
Goodwin, P., 2004. Analytical Solutions for Estimating Effective Discharge. J. Hydraul. Eng. 130, 729–738.
Guneralp, I., Marston, R.A., 2012. Process-form linkages in meander morphodynamics: Bridging theoretical modeling and real world complexity. Prog. Phys. Geogr. 36, 718–746.
Hanson, G.J., Simon, A., 1980. Erodibility of cohesive streambeds in the loess area of the midwestern USA. Hydrol. Process. 15, 23–38.
Hasan, M.A., Islam, A., Akanda, A.S., 2018. Climate projections and extremes in dynamically downscaled CMIP5 model outputs over the Bengal delta: a quartile based bias-correction approach with new gridded data. Clim Dynam. 51, 2169–2190.
Hicks, D.M., 1994. Land-use effects on magnitude-frequency characteristics of storm sediment yields: some New Zealand examples. IAHS Publ. 224, 395–402.
Hicks, D.M., Gomez, B., Trustrum, N.A., 2004. Event suspended sediment characteristics and the generation of hyperpycnal plumes at river mouths: east coast continental margin, North Island, New Zealand. J. Geol. 112, 471–485.
Hooke, J.M., 2015. Variations in flood magnitude-effect relations and the implications for flood risk assessment and river management. Geomorphology 251, 91–107.
Kang, S., et al., 2010. Review of climate and cryospheric change in the Tibetan Plateau. Environ. Res. Lett. 5, 015101.
Karmaker, T., Dutta, S., 2015. Stochastic erosion of composite banks in alluvial river bends. Hydrol. Process. 29, 1324–1339.
Klavon, K., et al., 2017. Evaluating a process-based model for use in streambank stabilization: insights on the Bank Stability and Toe Erosion Model (BSTEM). Earth Surf. Process. Landf. 42, 191–213.
Knighton, D., 1998. Fluvial Forms & Processes. A New Perspective Arnold, London.
Konsuer, K.M., et al., 2016. Spatial variability in bank resistance to erosion on a large meandering, mixed bedrock-alluvial river. Geomorphology 252, 80–97.
Lai, Y.G., et al., 2015. Modeling of multilayer cohesive bank erosion with a coupled bank stability and mobile-bed model. Geomorphology 243, 116–129.
Lenzi, M.A., Mao, L., Comiti, F., 2006. Effective discharge for sediment transport in a mountain river: Computational approaches and geomorphic effectiveness. J. Hydrol. 326, 257–276.
Leopold, L.B., Wolman, W.G., Miller, J.P., 1964. Fluvial processes in geomorphology. W. H Freeman and Company, San Francisco.
Li, D.F., Li, Z.W., Zhou, Y.J., Lu, X.X., 2020. Substantial Increase in the water and sediment fluxes in the headwater region of the Tibetan Plateau in response to global warming. Geophys. Res. Lett. 47, e2020GL087745.
Li, Z.W., Gao, P., 2019a. Channel adjustment after artificial neck cutoffs in a meandering river of the Zoige basin within the Qinghai-Tibet Plateau, China. Catena 172, 255–265.
Li, Z.W., Gao, P., 2019b. Impact of natural gullies on groundwater hydrology in the Zoige peatland, China. J. Hydrol. Regional Stud. 21, 25–39.
Lotsari, E.S., et al., 2018. Topographical change caused by moderate and small floods in a gravel bed ephemeral river – a depth-averaged morphodynamic simulation approach. Earth Surf. Dynami. 6, 163–185.
Luppi, L., Rinaldi, M., Teruggi, L.B., Darby, S.E., Nardi, L., 2009. Monitoring and numerical modelling of riverbank erosion processes: a case study along the Cecina River (central Italy). Earth Surf. Process. Landf. 34, 530–546.
Magilligan, F.J., Buraas, E.M., Renshaw, C.E., 2015. The efficacy of streampower and flow duration on geomorphic responses to catastrophic flooding. Geomorphology 228, 175–188.
Masoodi, A., Tabatabai, M.R.M., Noorzad, A., Samadi, A., 2019. Riverbank Stability under the Influence of Soil Dispersion Phenomenon. J. Hydrol. Eng. 24 (3), 05019001.
McCuen, R., 2004. Hydrologic analysis and design. Pearson Prentice Hall, Upper Saddle River, New Jersey.
Mecklenburg, D., 2006. Division of Soil and Water Conservation: STREAM Modules. Retrieved 10 1. Ohio Department of Natural Resources, Columbus.
Meyer, G.A., 2001. Recent large-magnitude floods and their impact on valley-floor environments of northeastern Yellowstone. Geomorphology 40, 271–290.
Micheli, E.R., Kirchner, J.W., 2002. Effects of wet meadow riparian vegetation on streambank erosion. 2. Measurements of vegetated bank strength and consequences for failure mechanics. Earth Surf. Process. Landf. 27, 687–697.
Midgley, T.L., Fox, G.A., Heeren, D.M., 2012. Evaluation of the bank stability and toe erosion model (BSTEM) for predicting lateral retreat on composite streambanks. Geomorphology 145, 107–114.
Motta, D., Langendoen, E.J., Abad, J.D., Garcia, M.H., 2014. Modification of meander migration by bank failures. J. Geophys. Res. Earth Surf. 119, 1026–1042.
Parker, G., et al., 2011. A new framework for modelling the migration of meandering rivers. Earth Surf. Process. Landf. 36, 70–86.
Patsinghasanee, S., Kimura, I., Shimizu, Y., Nabi, M., 2018. Experiments and modelling of cantilever failures for cohesive riverbanks. J. Hydrau. Res. 56, 76–95.
Phillips, J.D., 2002. Geomorphic impacts of flash flooding in a forested headwater basin. J. Hydrol. 269, 236–250.
Rinaldi, M., Casagli, N., Dapporto, S., Gargini, A., 2004. Monitoring and modelling of pore water pressure changes and riverbank stability during flow events. Earth Surf. Process. Landf. 29, 237–254.
Rinaldi, M., Mengoni, B., Luppi, L., Darby, S.E., Mosselman, E., 2008. Numerical simulation of hydrodynamics and bank erosion in a river bend. Water Resour. Res. 44, W09428. https://doi.org/10.1029/2008WR007008.
Rousseau, Y.Y., Van de Wiel, M.J., Biron, P.M., 2017. Simulating bank erosion over an extended natural sinuous river reach using a universal slope stability algorithm coupled with a morphodynamic model. Geomorphology 295, 690–704.
Roy, N.G., Sinha, R., 2014. Effective discharge for suspended sediment transport of the Ganga River and its geomorphic implication. Geomorphology 227, 18–23.
Samadi, A., Amiri-Tokaldany, E., Davoudi, M.H., Darby, S.E., 2011. Identifying the effects of parameter uncertainty on the reliability of modeling the stability of overhanging, multi-layered, river banks. Geomorphology 134, 483–498.
Samadi, A., Amiri-Tokaldany, E., Davoudi, M.H., Darby, S.E., 2013. Experimental and numerical investigation of the stability of overhanging riverbanks. Geomorphology 184, 1–19.
Schmidt, K., Morche, D., 2006. Sediment output and effective discharge in two small high mountain catchments in the Bavarian Alps, Germany. Geomorphology 80, 131–145.
Simon, A., Castro, J., Rinaldi, M., 2016. Channel form and adjustment: characterization, measurement, interpretation and analysis. In: Kondolf, G.M., Piégay, H. (Eds.), Tools in Fluvial Geomorphology. Wiley Blackwell, Chichester, UK, pp. 237–259.
Simon, A., Collison, A.J.C., 2001. Pore-water pressure effects on the detachment of cohesive streambeds: Seepage forces and matric suction. Earth Surf. Process. Landf. 26, 1421–1442.
Simon, A., Dickerson, W., Heins, A., 2004. Suspended-sediment transport rates at the 1.5-year recurrence interval for ecoregions of the United States: transport conditions at the bankfull and effective discharge? Geomorphology 58, 243–262.
Simon, A., Pollen-Bankhead, N., Thomas, R.E., 2011. Development and application of a deterministic bank stability and toe erosion model for stream restoration. In: Simon, A., Bennett, S.J., Castro, J.M. (Eds.), Stream restoration in dynamic fluvial systems. American Geophysical Union, Washington, D.C., pp. 453–474
Thompson, C., Croke, J., 2013. Geomorphic effects, flood power, and channel competence of a catastrophic flood in confined and unconfined reaches of the upper Lockyer valley, southeast Queensland, Australia. Geomorphology 197, 156–169.
Thorne, C.R., 1982. Processes and mechanisms of river bank erosion. In: Hey, R.D., Bathurst, J.C., Thorne, C.R. (Eds.), Gravel-Bed Rivers. John Wiley & Sons, Chichester, UK, pp. 227–271.
Thorne, C.R., Tovey, N.K., 1981. Stability of composite river bank. Earth Surf. Process. Landf. 6, 469–484.
Torizzo, M., Pitlick, J., 2004. Magnitude-frequency of bed load transport in mountain streams in Colorado. J. Hydrol. 290, 137–151.
Visconti, F., Camporeale, C., Ridolfi, L., 2010. Role of discharge variability on pseudomeandering channel morphodynamics: Results from laboratory experiments. J. Geophys. Res. Earth Surf. 115, F04042.
Wolman, M.G., Miller, J.P., 1960. Magnitude and frequency of forces in geomorphic processes. J. Geol. 68, 54–74.
Wyzga, B., Radecki-Pawlik, A., Galia, T., Plesinski, K., Skarpich, V., Dusek, R., 2020. Use of high-water marks and effective discharge calculation to optimize the height of bank revetments in an incised river channel. Geomorphology 356, 107098.
Xia, J.Q., Zong, Q.L., Deng, S.S., Xu, Q.X., Lu, J.Y., 2014. Seasonal variations in composite riverbank stability in the Lower Jingjiang Reach, China. J. Hydrol. 519, 3664–3673.
Xu, L.L., Wang, A., Wang, D., Wang, H.J., 2019. Hot Spots of Climate Extremes in the Future. J. Geophys. Res. Atmosph. 124, 3035–3049.
Yao, T., et al., 2012. Different glacier status with atmospheric circulations in Tibetan Plateau and surroundings. Nat. Clim. Change 2, 663–667.
Yellen, B., Woodruff, J.D., Cook, T.L., Newton, R.M., 2016. Historically unprecedented erosion from Tropical Storm Irene due to high antecedent precipitation. Earth Surf. Process. Landf. 41, 677–684.
Yu, M.H., Wei, H.Y., Wu, S.B., 2015. Experimental study on the bank erosion and interaction with near-bank bed evolution due to fluvial hydraulic force. Int. J. Sediment Res. 30, 81–89.
Zong, Q.L., Xia, J.Q., Zhou, M.R., Deng, S.S., Zhang, Y., 2017. Modelling of the retreat process of composite riverbank in the Jingjiang Reach using the improved BSTEM. Hydrol. Process. 31, 4669–4681.